R.L. Murty
Professor

M.A. Qayyum
Post-graduate Student

Mechanical Engineering,
Regional Engineering College,
Warangal, India

Application of MOIRE Technique to the Determination of Stresses on the Rake Surface of Single Point Cutting Tool Models

The stresses developed on the rake face of single point tool models under the action of a static force by applying MOIRE technique have been investigated. Three tool models with varying rake angles (+30, 0, and −30 deg) are studied and the stresses developed on the rake face are compared.

Introduction

Various investigators have conducted experiments while machining lead with a two-dimensional orthogonal tool made of a photoelastic material [1–3][1] with a view to evaluating the stress distribution on the rake surface of the tool. In most practical situations, however, the tool used is a complex three-dimensional object. The stresses developed on its rake face under the action of the cutting forces are extremely difficult to calculate theoretically. In the present work, an attempt is made to evaluate experimentally the stresses on the rake face of a single point tool model using the MOIRE technique [4–6].

Load Simulation

For a tool having $\lambda = 0$ deg and $\phi_r = 90$ deg, (according to the tool nomenclature recommended by CIRP) there are two components, P_z and P_y of the cutting force (P_z = main cutting force, P_y = feed force in a plane parallel to the basic plane of the tool and perpendicular to the main cutting edge), assuming free cutting. When a static load was applied on the tool model at the tool nose in the direction of the main cutting force P_z, no or very little change in the fringe pattern was noticed. This means, interestingly enough, that the stresses induced on the rake surfaces (except the contact stresses in a small region directly under the load) due to an external force in the direction of the main cutting force are negligible. Thus, it is considered sufficient to evaluate the stresses on the rake surface when the tool model is subjected to a load in a plane parallel to the basic plane of the tool model and in a direction perpendicular to the main cutting edge, that is, subjected to a load simulating the feed force. The loading arrangement is shown schematically in Fig. 1. "2" is a nut fixed in a vice "1" and carries a screw "3" with a handle. "4" is a U-type dynamometer with dial gauge "5." "6" is an aluminum tip, through which the load is applied onto the tool "8." The bush "7" prevents the rotation of the dynamometer and the aluminum tip while loading the tool.

Models of Tools

Tool models of 2 × 2 in. cross section and 8 in. long were made in Perspex, bonding four pieces of sheet, × ½ in. cross section and 8 in. long with Araldite. The clearance and rake surfaces of the tools were ground on a universal tool and cutter grinder. The geometry

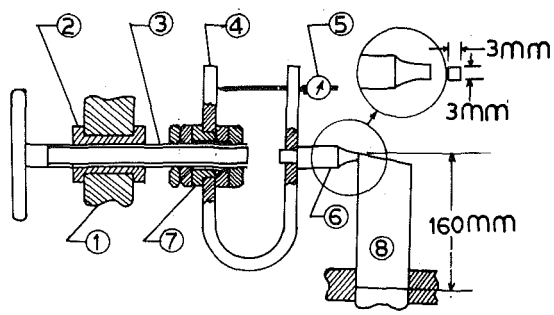

Fig. 1 Experimental setup (1—vice, 2—nut, 3—screw, 4—U-dynamometer, 5—dial gauge, 6—aluminum tip, 7—bush, 8—tool)

[1] Numbers in brackets designate References at end of paper.

Contributed by the Production Engineering Division for publication in the JOURNAL OF ENGINEERING FOR INDUSTRY. Manuscript received at ASME Headquarters July 1, 1975. Paper No. 75-Prod-M.

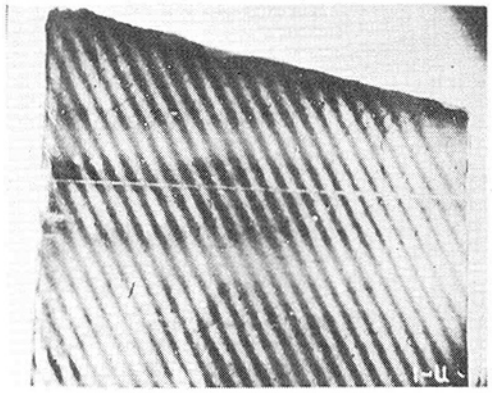

Fig. 2 U-MOIRE, initial mismatch (Model 1)

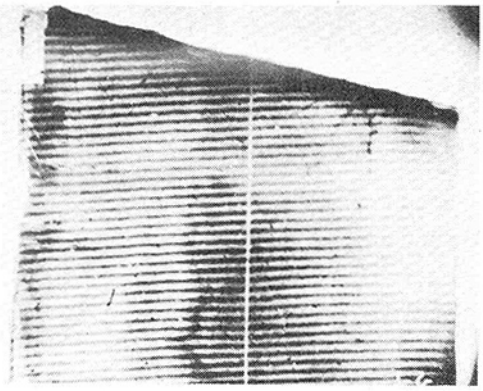

Fig. 3 V-MOIRE, initial mismatch (Model 2)

of the three tools tested is given in Table 1. The values of the rake angles chosen are large in comparison with the ones used in practice; but this has been done intentionally to intensify the effect of any changes that are likely to occur in the stress pattern on the rake face with changing rake angles.

Orthogonal MOIRE gratings of line density, 24 lines/mm, were fixed onto the rake face of the tools by the use of Eastman 910, a special adhesive supplied by the Eastman Kodak Company, U.S.A. The fixing was done in the National Physical Laboratory, New Delhi.

Experimental Procedure

The tool model was fixed in the vice as shown in Fig. 1. A suitable camera (supplied along with the Chapman Polariscope) with a magnification ×2 was adjusted so that its axis is perpendicular to the plane of interest, that is, the rake surface. In the unstressed condition two photographs were taken, one with the master grid lines parallel to the main cutting edge and the second with the master grid line perpendicular to the main cutting edge. To facilitate this, a thin line is drawn with a scriber on the master grid while the magnified master grid is observed on an inspection enlarger so that the line is parallel to the master grid lines. This can be seen as a white line on all the photographs. Having taken the two photographs of the MOIRE pattern in the instrained condition, the model was loaded to 40 kg in the direction of the feed force. In this position two more photographs of the MOIRE pattern were taken just as in the unstressed condition. Linear compressive and rotational mismatches were used to increase the accuracy of calculation. The magnitude of the mismatches was calculated later from the displacement curves obtained from the initial MOIRE pattern in the unstressed condition.

Method of Calculation

The photographs of the MOIRE fringes for the Model 1 are shown in Figs. 2–5. Fig. 6 indicates the directions of the coordinate axes and the positions of the points for which the stresses were calculated. The photographs in which the white line is perpendicular to the main cutting edge yield the displacement and those in which the white line is parallel to the main cutting edge yield the displacement V. The construction of the displacement diagrams from the MOIRE patterns is discussed in the references [4, 5]. Two such displacement curves (for Model 1) are shown in Figs. 7 and 8.

The slopes of the displacement curves at the points of interest give the strains. Since an initial mismatch was used, the strain, at a point, will be given by

$$\epsilon = \tan\alpha - \tan\beta \tag{1}$$

where

α = slope of the displacement curve at the point of interest in the stressed model

β = slope of the displacement curve at the point of interest in the unstressed model, viz., due to the initial mismatch

The slopes can be obtained either graphically or by numerical methods. Some of the strains depending upon the need have been calculated by fitting a suitable empirical equation to the displacement curves and obtaining the slope by differentiating this equation. The normal strains in the two coordinate directions are given by

$$\epsilon_x = \frac{\partial u}{\partial x} \tag{2}$$

$$\epsilon_y = \frac{\partial v}{\partial y} \tag{3}$$

The shearing strain is given by

$$\gamma_{xy} = \frac{\partial u}{\partial y} + \frac{\partial v}{\partial x} \tag{4}$$

Once the two normal strains and the shearing strain at a point are shown, the principal strains ϵ_1 and ϵ_2 are evaluated by the construction of the Mohr's Circle.

The normal stresses σ_x and σ_y are obtained from the following equations:

$$\sigma_x = \frac{E(\epsilon_x + \mu\epsilon_y)}{(1-\mu^2)} \tag{5}$$

$$\sigma_y = \frac{E(\epsilon_y + \mu\epsilon_x)}{(1-\mu^2)} \tag{6}$$

Nomenclature

ϕ_r = major cutting edge angle
ϕ_r' = minor cutting edge angle
α_n = normal clearance angle (major cutting edge)
α_n' = normal clearance angle (minor cutting edge)
λ = cutting edge inclination
γ_n = normal rake angle
ϵ = strain
ϵ_1, ϵ_2 = principal strains
ϵ_x, ϵ_y = normal strains
σ_1, σ_2 = principal stresses
σ_x, σ_y = normal stresses
E = Young's modulus
μ = Poisson ratio
u = component of displacement in the x-direction
V = component of displacement in the y-direction
γ_{xy} = shearing strain
τ_{max} = maximum shearing stress

Table 1 Geometry of the tools tested

	ϕ_r (deg)	ϕ_r' (deg)	α_n (deg)	α_n' (deg)	λ (deg)	γ_n (deg)
Tool 1	90	10	8	8	0	+30
Tool 2	90	10	8	8	0	0
Tool 3	90	10	8	8	0	−30

The principal stresses σ_1 and σ_2 are obtained from the following equations:

$$\epsilon_1 = \frac{1}{E}(\sigma_1 - \mu\sigma_2) \tag{7}$$

$$\epsilon_2 = \frac{1}{E}(\sigma_2 - \mu\sigma_1) \tag{8}$$

The values of E and μ for the model material are 1.45×10^4 kg/cm^2 and 0.3, respectively.

Results and Discussion

The principal stresses and the maximum shear stress at the various points on the rake face for the tool models 1, 2, and 3 are indicated compactly in Table 2. The "isobars" or contours of constant normal stresses (σ_x and σ_y) are given in Figs. 9–14. The isobars of normal stresses only are plotted as the MOIRE technique intrinsically makes possible a more accurate determination of normal stresses than the shearing stresses. The determination of the shearing stresses is necessarily less accurate owing to the absence of symmetry about any axis in the tool models. The absence of the axis of symmetry makes the angular alignment of the master grid with respect to the model grid difficult.

It has not been possible to find the stresses at the edge of the models. This is due to the following: (1) It has not been possible to fix the master right at the edges, as the applied load will disturb its position. (2) Owing to the sloping clearance faces, the incident light gets partly reflected at the edges and produces a dark region very near to the cutting edge. For these reasons the stresses obtained are only for a region which is 2.5 mm away from both the edges.

An examination of the normal stress contours helps to arrive at the following conclusions: (1) All the models have a distinct zone of zero stress surrounded by regions of compressive and tensile stresses, except for σ_y of Model 1 (with γ_n = +30 deg). (2) The stress contours in Model 3 are irregular. This may be because the interface between two constituent pieces (the tool model was built by gluing four pieces together) appeared very near to the cutting edge, viz., at about the section 2y, distant 5 mm

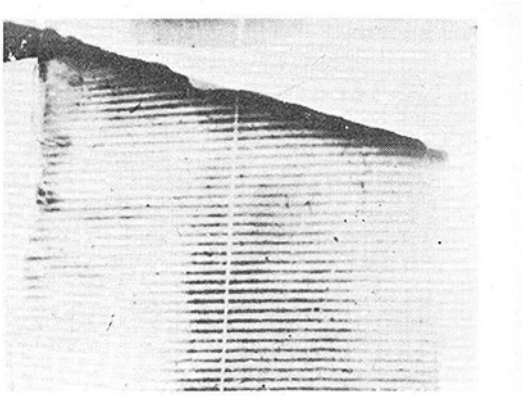

Fig. 5 V-MOIRE, initial mismatch and load of 40 kg (Model 1)

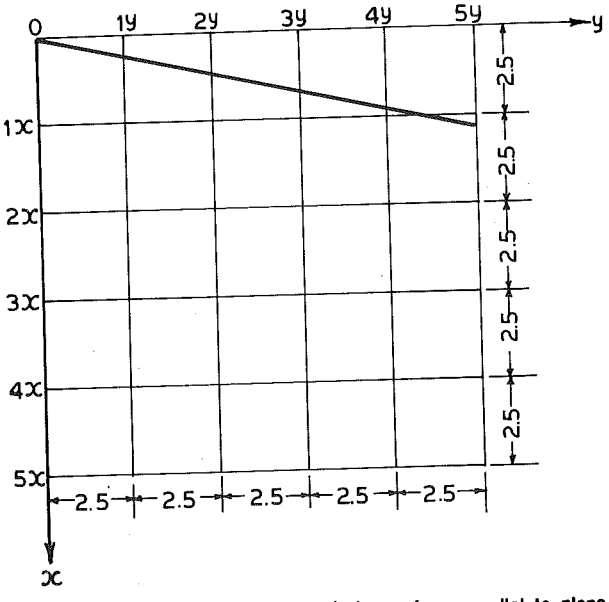

Fig. 6 Coordinate axes of the tool (rake surface parallel to plane of paper, dimensions in mm)

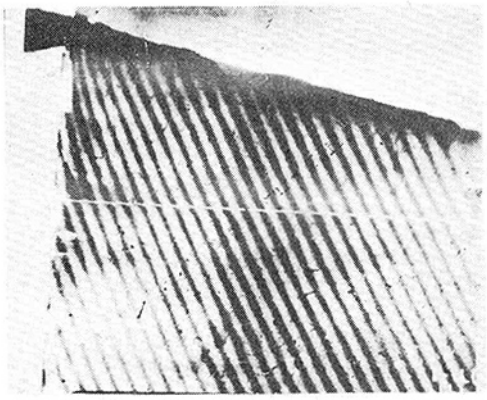

Fig. 4 U-MOIRE, initial mismatch and load of 40 kg (Model 1)

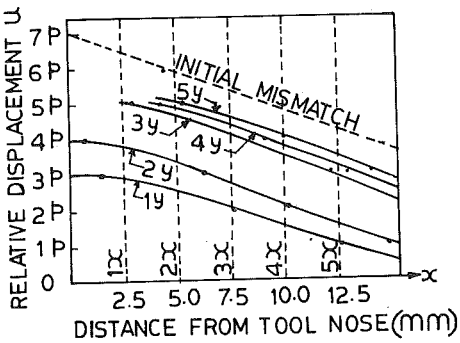

Fig. 7 Displacement curve, u against x for Model 1 (p—pitch of the master grid)

Table 2 Principal stresses and maximum shearing stresses (kg/cm²)

	0		1y		2y		3y		4y	
	+53.3	-45.0	+37.3	-49.9	+48.5	-46.2	+48.5	-45.9	+48.6	-46.0
	-36.0	-120.0	-31.6	-105.2	-26.8	-89.3	-22.0	-73.4	+17.2	-57.1
	-9.7	-32.4	+109.0	-8.0	+126.5	-14.35	+36.5	-51.5	-80.9	-97.0
1x										
	49.15		43.6		47.35		47.2		47.3	
	42.00		36.8		31.25		25.7		20.0	
	11.35		58.5		70.43		44.0		8.0	
	+24.9	-62.2	+23.5	-110.5	+37.8	-91.8	+50.2	-79.2	+42.0	-58.5
	+15.9	-9.7	+5.6	-34.6	+1.8	-54.6	+55.7	-68.0	-14.1	-71.0
	-25.2	-87.5	+61.6	-22.2	+65.2	+13.7	+30.3	+89.0	-4.9	+95.0
2x										
	43.5		67.0		64.8		64.7		50.3	
	12.8		20.1		28.2		36.9		42.5	
	30.7		41.9		25.8		29.4		49.9	
	+10.2	-57.8	+4.0	-78.8	+0.6	-75.6	-2.9	-67.5	-14.8	-56.7
	+28.4	+60.7	-5.6	+41.9	+17.1	-25.4	-0.6	-43.0	-18.0	-65.0
	-11.6	-38.6	+20.8	-22.8	-10.4	-39.4	+14.6	-38.4	+46.3	-15.2
3x										
	34.00		41.35		37.97		32.32		20.90	
	16.15		23.74		21.25		21.22		23.50	
	13.50		21.70		14.50		26.50		30.70	
	+4.6	-23.3	-7.8	-35.8	-1.1	-42.4	-4.6	-36.9	-10.3	-33.5
	+30.6	-6.8	+5.0	+4.4	-9.9	+20.3	-9.9	+20.3	-2.8	+17.3
	-1.4	-4.6	-35.7	-7.8	-104.0	-26.8	-47.5	+6.1	+72.2	-8.6
4x										
	14.0		14.0		20.6		16.2		11.6	
	18.7		0.2		15.1		15.1		10.0	
	1.6		14.0		38.6		26.8		40.4	
	+17.9	-34.0	-10.3	-34.3	-9.6	-31.9	-10.7	-30.8	-9.34	-31.1
	-37.6	-14.9	+3.4	-3.4	+14.5	-14.5	+12.75	-10.7	+7.0	-8.1
	+23.9	-0.1	-73.1	-19.1	-184.0	+59.5	-68.8	-9.6	-106.0	+25.9
5x										
	25.9		10.0		11.2		10.1		10.4	
	26.2		0		0		11.7		7.5	
	12.0		27.0		122.0		29.4		39.9	

σ_1

Model 1
Model 2
Model 3

σ_2

Model 1
Model 2
Model 3

τ max

Model 1
Model 2
Model 3

Magnitudes of principal and shearing stresses for the various models

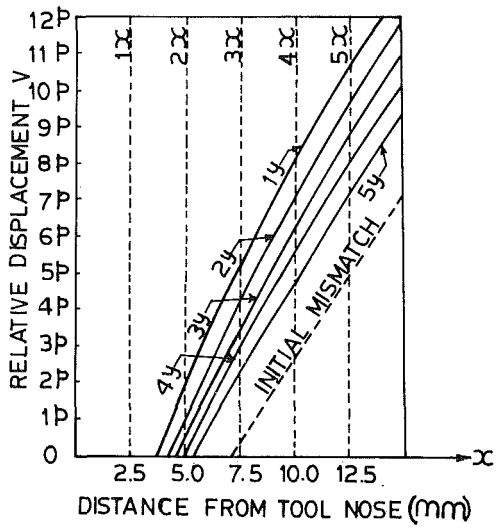

Fig. 8 Displacement curve, *V* against *x* for Model 1 (*p*—pitch of the master grid)

from the cutting edge.

In addition, Figs. 9–14 and Table 2 reveal that the stresses do not fall uniformly from the region of the tool corner in either direction. This is contrary to what may be expected. Owing to the complex interaction of various effects—viz., stresses of a wedge under compression, wedge under bending, contact stresses, beam stresses, etc.—the stress distribution on the rake face is complex with the existence of tensile, compressive, and zero stress zones.

The magnitudes of the greatest stresses in the three models are given in Table 3. The table shows that the tool Model 3 ($\gamma_n = -30$ deg) leads to the highest magnitude of all the stresses. The tensile stresses in Models 1 and 2 are almost equal, whereas the shear stress in Model 2 is much smaller than in Models 1 and 3. Though

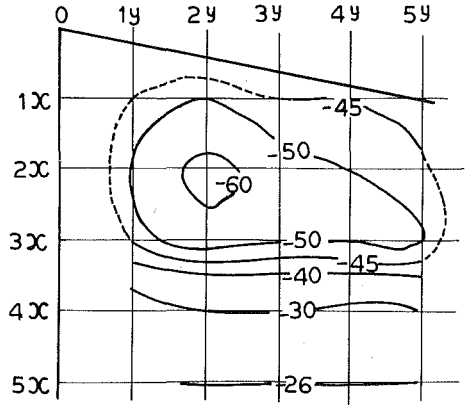

Fig. 9 σ_y contours (Model 1) (stress in kg/cm²)

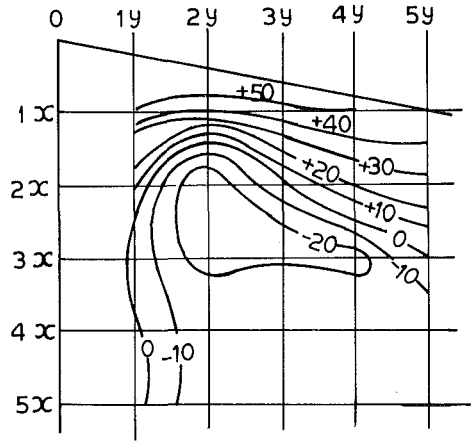

Fig. 10 σ_x contours, Model 1

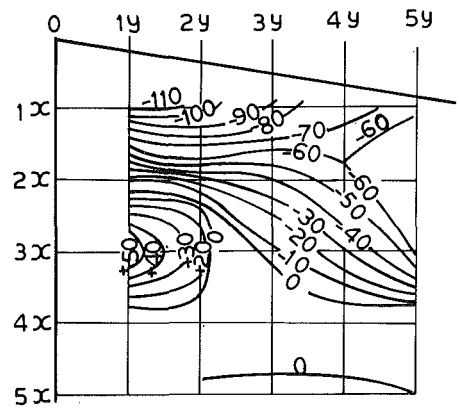

Fig. 11 σ_y contours, Model 2

Table 3 Magnitudes of the greatest stress on the models

Model No.	Greatest value of normal stress (kg/cm²) Compressive	Greatest value of normal stress (kg/cm²) Tensile	Greatest value of principal stress (kg/cm²) Compressive	Greatest value of principal stress (kg/cm²) Tensile	Greatest value of shearing stress (kg/cm²)
1 (γ_n = +30 deg)	−60	+50	−110	+55	67
2 (γ_n = 0 deg)	−120	+60	−120	+60	42
3 (γ_n = −30 deg)	−180	+125	−185	+125	122

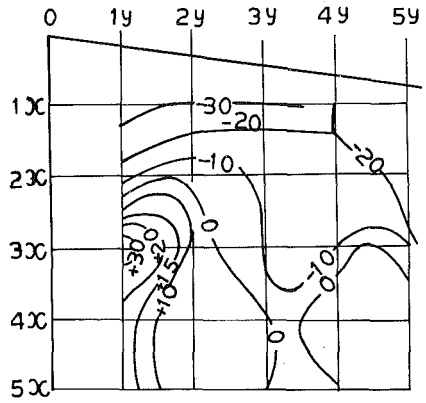

Fig. 12 σ_x contours, Model 2

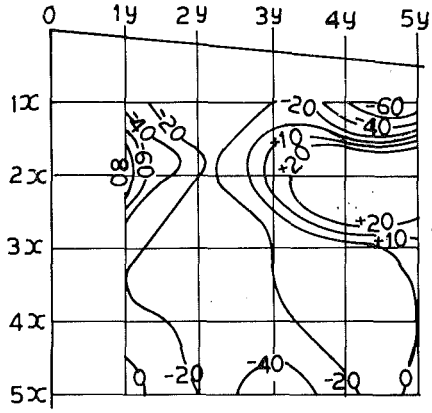

Fig. 13 σ_y contours, Model 3

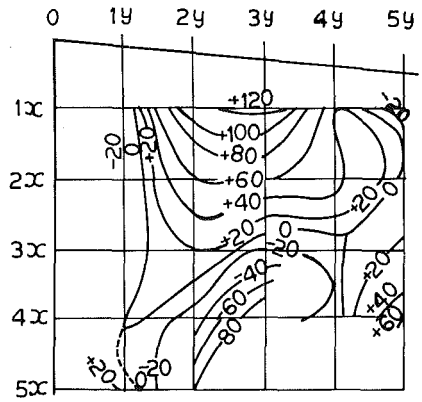

Fig. 14 σ_x contours, Model 3

the magnitude of the greatest tensile stress is highest in the case of Model 3, and in Models 1 and 2 almost equal, it is necessary to remember that the region of tensile stresses occurs very near to the tool nose in Model 1, whereas it is away from the tool nose in Models 2 and 3. These observations reveal that tool 2 (γ_n = 0 deg) has the most favorable stress state and tools with zero and negative rake angles have regions of compressive stresses near the tool nose.

This discussion reveals that the tools with zero and negative rakes have a more favorable stress state, in that they have compressive stresses occurring near the tool nose and the tool with zero rake has the smallest magnitude of shearing stresses. This observation is very interesting and seems to justify the provision of rake angles around zero and small negative rake angles on carbide and ceramic tools.

The results of this work may be held at a discount at this stage, until they are corroborated by further theoretical or experimental work. At present they are not connected with existing theoretical or experimental knowledge. While admitting such a deficiency, the attention of the reader is drawn to the following features of the nature of the work: (*a*) the displacement curves are smooth, and (*b*) the normal stress contours are consistent. This shows that the obtained stresses faithfully represent the stress pattern under the given loading conditions and proves that MOIRE technique can be used for the determination of stresses on the face of a complex three-dimensional body as a single point tool.

Acknowledgment

The help rendered by Dr. V. Venkateswara Rao, Professor of Physics, in arranging the help by the National Physical Laboratory for the present work deserves to be mentioned.

References

1 Usui, E., and Takeyama, H., "A Photo-Elastic Analysis of Machining Stress," JOURNAL OF ENGINEERING FOR INDUSTRY," TRANS. ASME, Vol. 82, 1960, p. 303.

2 Chandrasekharan, H., and Kapoor, D. V., "Photo-Elastic Analysis of Tool-Chip Interface Stresses," JOURNAL OF ENGINEERING FOR INDUSTRY, TRANS. ASME, Vol. 87, 1965, p. 495.

3 Amini, E., "Photo-Elastic Analysis of Stresses and Forces in Steady Cutting," *Journal of Strain Analysis*, Vol. 3, No. 3, 1968.

4 Seiammarella, C. A., and Durelli, A. J., "Moire Fringes as a Means of Analysing Strains," *Transactions of the ASCE*, Vol. 27, Part I, 1962.

5 Agarwala, B. K., Harsh Vardhan, Bindal, M. M., and Rakesh Kumar, "Lecture Notes on Moire Technique in the Measurement of Linear and Angular Displacements," Special Summer Institute, 1970 (National Physical Laboratory, New Delhi).

6 Fue-Pen Chaiang, "Determination of Signs in Moire Method," *Proceedings of the ASCE, Journal of the Engineering Mechanics Division*, Vol. 95, Dec. 1969.